Cone beam CT dosimetry: A unified and self-consistent approach including all scan modalities—With or without phantom motion

Robert L. Dixon[a)]
Department of Radiology, Wake Forest University School of Medicine, Winston-Salem, North Carolina 27160

John M. Boone
Department of Radiology, University of California Davis Medical Center, Sacramento, California 95817

(Received 3 January 2010; revised 24 February 2010; accepted for publication 24 March 2010; published 19 May 2010)

Purpose: This article describes a common methodology and measurement technique, encompassing both conventional (helical and axial) CT scanning *using phantom translation* and cone beam (or narrow fan beam) CT scans *about a stationary phantom*. Cone beam CT systems having beam widths along the z-axis wide enough to cover a significant anatomical length (50–160 mm) in a single axial rotation (e.g., in cardiac CT) are rapidly proliferating in the clinic, referred to herein as stationary cone beam CT (SCBCT). The integral format of the CTDI paradigm is not appropriate for a stationary phantom, and is not useful for predicting the dose in SCBCT, nor for perfusion studies or CT fluoroscopy. Likewise, the pencil chamber has limited utility in this domain (even one of extended length).

Methods: By demonstrating, both experimentally and theoretically, the match between the dose distribution $f(z)$ for a wide cone beam and that due to an axial scan series $\tilde{D}(z)$, it is shown that the dose on the central ray of the cone beam $f(0)$ is both spatially colocated and numerically equal to the dose predicted by CTDI for the axial series; and thus $f(0)$ is the logical (and unique) choice for a SCBCT dose-descriptor consistent with the CTDI-based dose of conventional CT. This dose $f(0)$ can be readily measured using a conventional (short) ionization chamber. Additionally, Monte Carlo simulations of Boone [J. M. Boone, "Dose spread functions in computed tomography: A Monte Carlo study," Med. Phys. **36**, 4547–4554 (2009)], expressed as a scatter LSF (or DSF), allow the application of a convolution-based model [R. L. Dixon, M. T. Munley, and E. Bayram, "An improved analytical model for CT dose simulation with a new look at the theory of CT dose," Med. Phys. **32**, 3712–3728 (2005)] of the axial dose profile $f(z)$ for any primary beam width a (any $n \times T$), fan beam and cone beam alike, from a single LSF kernel; its simple form allows the results to be expressed as simple analytical equations. The experimental data of Mori *et al.* [S. Mori, M. Endo, K. Nishizawa, T. Tsunoo, T. Aoyama, H. Fujiwara, and K. Murase, "Enlarged longitudinal dose profiles in cone-beam CT and the need for modified dosimetry," Med. Phys. **32**, 1061–1069 (2005)] from a 256 channel cone beam scanner for a variety of beam widths (28–138 mm) are used to corroborate the theory.

Results: Useful commonalities between SCBCT and conventional CT dose are revealed, including a common equilibrium dose parameter A_{eq}, which is independent of z-collimator aperture a (or $n \times T$), and a common analytical (exponential growth) function $H(\lambda)$ describing the relative approach to scatter equilibrium at $z=0$ for both modalities (with $\lambda = a$ or $\lambda =$ scan length L). This function exhibits good agreement with the above-mentioned cone beam data of Mori *et al.* for $H(a)$ as well as with data $H(L)$ obtained from conventional CT scanning [R. L. Dixon and A. C. Ballard, "Experimental validation of a versatile system of CT dosimetry using a conventional ion chamber: Beyond $CTDI_{100}$," Med. Phys. **34**(8), 3399–3413 (2007)] for the same directly irradiated, phantom length $L=a$.

Conclusions: This methodology and associated mathematical theory provide a physically self-consistent description of dose between stationary phantom CT and conventional CT, and has predictive capabilities which can be used to effect a substantial reduction in data collection; provide a bridge between modalities; and predict the relevant peak doses $f(0)$ for perfusion studies. © *2010 American Association of Physicists in Medicine*. [DOI: 10.1118/1.3395578]

I. INTRODUCTION

CT systems having beam widths along the z-axis wide enough to cover a significant anatomical length in a single axial rotation are rapidly proliferating in the clinic. Some utilize a conventional CT platform and can provide both conventional helical or axial scanning motions involving patient/table translation, as well as single (or multiple) rotation acquisitions at a fixed z location without table motion (used, for

example, in acquiring cardiac images using subsecond scans), having selectable nominal cone beam widths of 40–160 mm in one 320 channel system recently introduced. The methodology introduced herein for stationary phantom cone beam CT (SCBCT) also applies to any CT scan without table motion (whether wide cone beam or narrow fan beam) in applications ranging from CT fluoroscopy, brain perfusion, and multiphasic liver scans.

A primary objective of this paper is the description of a self-consistent methodology which can bridge the gap between the dose accrued in conventional helical or axial scan modes in which the phantom is translated through a distance L; and CT operation without table/phantom motion, usually (but not necessarily) utilizing wider "cone beams" having variable lengths of 40–180 mm along z.

The experimental data of Mori *et al.*[1] obtained on a 256 channel cone beam CT scanner (the prototype of the above-mentioned 320 channel scanner) are used to corroborate the theory and conclusions. This system and data set are also representative of the commercially available 320 channel system; the basic principles are unchanged.

For brevity, the two modalities are referred to as

A. "Conventional CT." Axial or helical scan acquisitions using multiple rotations, regularly spaced along z due to table/phantom translation over $(-L/2, L/2)$.

B. "SCBCT." Image data are acquired using single or multiple axial rotations about a stationary phantom (table advance $b=0$, scan length $L=0$). (The results are also applicable to narrow "fan beam" CT using a stationary phantom as used in perfusion studies).

It will be shown in Sec. II that the dose on the central ray of the cone beam $f(0)$ is both spatially colocated and numerically equal to the dose predicted by CTDI for a conventional scan series; and thus $f(0)$ is the logical (and unique) choice for a SCBCT dose-descriptor consistent with the CTDI-based dose used in conventional CT. In addition to a common mathematical formalism which describes the dose for both modalities, there is an identical measurement technique applicable to both cases utilizing a short ionization chamber.[2]

Both modalities are shown to possess a common equilibrium dose parameter A_{eq} which is independent of z-collimator aperture a (or $n\times T$), and a common analytical function $H(\lambda)$ is derived describing the relative approach to scatter equilibrium at $z=0$ (with $\lambda=a$ for the stationary phantom or $\lambda=$scan length L). This commonality provides a crossover or bridge between conventional and stationary phantom CT, such that one can predict the complete data set for both modalities from a single measurement of the central (peak) dose $f(0)$ resulting from a single axial rotation at a given aperture setting a. From this, one can predict the SCBCT or fan beam peak dose $f(0)$ for any beam width a, and the conventional CT dose (as predicted by CTDI) for any scan length L (including the limiting equilibrium dose) for any collimator aperture setting a and any pitch p. Although the crossover between modalities is an interesting aspect of the theory developed, it is by no means the only application or goal of the theoretical development to follow.

The glossary of parameters in the Appendix is provided as a quick reference for the following development and throughout.

The following development concentrates on the *actual in-phantom dose* for both conventional CT involving phantom translation, and stationary phantom CT such as SCBCT, directed toward creating a consistent approach to CT dose assessment which provides continuity of dose and physical interpretation between these two modalities. To that end, it is necessary to review the dose-descriptors used in conventional CT (and the CTDI paradigm).

II. THEORY

II.A. Conventional CT scanning using table/phantom translation

II.A.1. Accumulated dose equations for helical or axial scan trajectories utilizing table/phantom translation along z

The best way to establish the correct and unequivocal physical interpretation (and limitations) of the CTDI equation and its related dose equations *is to derive it*. A simpler derivation[3] (compared to the original[4]) using convolution methods is outlined below (the resulting equations are also necessary and pertinent to this paper).

II.A.1.a. Axial scanning. One assumes a series of $N=2J+1$ rotations, each producing an identical axial dose profile $f(z)$ centered at $z'=kb$ (where k denotes the k_{th} rotation); spaced at *equal intervals* b; and dispersed over a total phantom length $L=Nb$ along z as a result of translating the table (and phantom) by a distance b between each rotation ("step and shoot"). This results in a quasiperiodic (or oscillatory) dose distribution[3] of fundamental period b, given by the superposition of displaced profiles shown below

$$\tilde{D}_N(z)=\sum_{k=-J}^{J} f(z-kb)=f(z)\otimes\sum_{-J}^{J}\delta(z-kb), \tag{1}$$

also expressed above as the convolution of $f(z)$ with a finite "comb" of δ-functions, which replicate $f(z)$ at each location $z'=kb$. This assumes "shift-invariance" along z (identical dose profiles at each $z'=kb$ spaced at equal intervals b), which also requires a shift-invariant phantom having a constant cross-section and composition along z (including, but not restricted to, uniform cylindrical or elliptical phantoms). The pencil chamber measurement method is likewise foiled by any loss of shift-invariance.

This dose can be smoothed[3] by taking the "running mean" (averaging over $z\pm b/2$ at each z), which is equivalent to convolving Eq. (1) with the unit-area rect function $b^{-1}\Pi(z/b)$, which in turn collapses the δ-function comb into the longer rect function $\Pi(z/L)$ of length $L=Nb$; resulting in the convolution equation[3] for the smoothed dose $D_L(z)$ accumulated at each value of z for a scan length L and given by Eq. (2) below

$$D_L(z) = \frac{1}{b} f(z) \otimes \Pi(z/L) = \frac{1}{b} \int_{-L/2}^{L/2} f(z - z')dz', \quad (2)$$

where $f(z)$ includes both the primary beam and scatter contributions $f(z)=f_p(z)+f_s(z)$ and is therefore much broader than the *primary beam width* (FWHM) a, where a is equal to the z-collimator aperture geometrically projected onto the axis of rotation (AOR).[5] MDCT requires that $a>nT$ in order to keep the penumbra beyond the active detector length nT. Evaluation of Eq. (2) at $z=0$ results in the accumulated dose $D_L(0)$ *at the center of the scan length* L as given by Eq. (3) below

$$D_L(0) = \frac{1}{b} \int_{-L/2}^{L/2} f(z')dz', \quad (3)$$

which (for axial scans) represents an average dose over the small interval $\pm b/2$ about $z=0$, where b is typically small compared to the total scan length $L=Nb$.[6] Note, however, the implicit dependence of the integration limits $\pm L/2$ and the divisor b, physically related by $L=Nb$. We are now done. These three equations provide the complete physical basis for conventional CT dosimetry. The derivation of Eq. (3) outlined above is equivalent to the original derivation,[4] which led to the definition of MSAD and CTDI.

Equation (3) for $D_L(0)$ represents the basic equation upon which the CTDI methodology is based, in which the divisor b of the integral physically represents a table advance per rotation, with CTDI_L itself defined[4] as the value of $D_L(0)$ in Eq. (3), resulting from a specific table increment (scan interval) $b=nT$, which interval produces "contiguous" axial scans in the image domain (leaving no gaps in the *acquired image data*). Thus, physically, CTDI_L is equal to the *accumulated dose* at the center ($z=0$) of the scan length $(-L/2, L/2)$, for a table advance $b=nT=$"$N\times T$" (a generalized pitch $p=b/nT=1$). Substituting $b=nT$ into Eq. (3) gives the familiar CTDI equation

$$\mathrm{CTDI}_L = \frac{1}{nT} \int_{-L/2}^{L/2} f(z')dz', \quad (4)$$

which one can also express in terms of $D_L(0)$ from Eq. (3) and pitch p as $\mathrm{CTDI}_L=(b/nT)D_L(0)=pD_L(0)$.[6–8]

There is actually no imperative to have a separate equation for CTDI_L, since it simply represents a special case of Eq. (3), namely, a particular value of $D_L(0)$ corresponding to a specific table increment $b=nT$ (a pitch of unity), and thus nT in the CTDI equation *physically* represents a table increment.

Measurement of the integral in Eqs. (3) and (4) using a pencil chamber of fixed-length ℓ only allows prediction of the accrued dose at $z=0$ for a scan length $L=\ell$ (e.g., $L=100$ mm as for CTDI_{100}). Additionally, assigning a fixed integration length L (e.g., 100 mm) to CTDI_L breaks the required coupling $L=Nb$ between the divisor b and the integration limits $\pm L/2$. For conventional CT, as L becomes large enough to completely span the very long scatter tails of $f(z)$ at $L=L_{\mathrm{eq}}$, such that no additional scatter can reach $z=0$ for $L\geq L_{\mathrm{eq}}$ (symbolically $L\to\infty$), then $D_L(0)$ approaches its limiting value, the equilibrium dose D_{eq}, written as

$$D_{\mathrm{eq}}(a/b) = \frac{1}{b} \int_{-\infty}^{\infty} f(z')dz' \propto (a/b). \quad (5)$$

Since D_{eq} depends (explicitly) on the inverse of table increment b, and is directly proportional to the collimator aperture a implicitly through the infinite integral of $f(z)$ (as shown in Sec. III B), then D_{eq} is directly proportional to a/b.

II.A.1.b. Helical scanning. Equations (2)–(5) have likewise been shown[3] to apply to helical scanning at a pitch $p=b/nT$ if an *angular average* over 2π *at a fixed* z is used to smooth (average) the peripheral axis dose distribution rather than the longitudinal running mean used for axial scans [the dose for helical scans on the phantom central axis is nonoscillatory, requiring no averaging, and is given by Eq. (2)]. The longitudinal and angular averages have been shown[5] to converge at values of z where dose equilibrium has been established.

The derivation of Eqs. (2)–(5) for helical scanning[3] is briefly outlined below, since it more clearly illustrates some important properties of $D_L(0)$ and CTDI_L. The dose rate on the central axis is independent of beam (gantry) angle θ, hence the *dose rate* profile is $\dot{f}(z)=\tau^{-1}f(z)$, where τ is gantry rotation time. Translation of the table and phantom at velocity v produces a dose rate profile in the phantom reference frame expressed as a traveling wave $\dot{f}(z,t)=\tau^{-1}f(z-vt)$, thus the dose accumulated at a given z as the profile travels by is given by the time integral of $\dot{f}(z,t)$ over the total "beam-on" time t_0, namely, $D_L(z)=\tau^{-1}\int_{-t_0/2}^{t_0/2} f(z-vt)dt$. Conversion to the spatial domain using $z'=vt$, scan length $L=vt_0$, and a table advance per rotation $b=v\tau$ (a pitch of $p=b/nT$), leads directly to the same convolution equation for $D_L(z)$ [Eq. (2)] previously derived for axial scans, and from which Eqs. (3)–(5) also follow as before; however, $D_L(0)$ and CTDI_L in the helical mode both refer to the dose *precisely* at $z=0$ (and likewise on the peripheral axis where an angular average[3] is used).

If the table and phantom remain stationary ($v=0$), the time integral of the dose rate $\dot{f}(z)=\tau^{-1}f(z)$ is simply $D_L(z)=(t_0/\tau)f(z)=Nf(z)$; likewise, in the limit $v\to 0$, $L=vt_0\to 0$, the integration limits $\pm L/2\to 0$; thus the integral format of Eqs. (2)–(4) collapse, and all converge smoothly to $Nf(z)$ or $Nf(0)$. Likewise, for axial scanning, setting the table increment to $b=0$ in Eq. (1) reduces the summation to $\tilde{D}_N(z)=Nf(z)$, and the integral format of Eqs. (2)–(4) for axial scanning [including Eq. (4) for CTDI_L] also collapse, converging to $Nf(z)$ or $Nf(0)$ in the limit $b\to 0$, $L=Nb\to 0$. This convergence is readily seen using Eq. (3). As L becomes very small, the integral can be approximated by $f(0)L$, thence $D_L(0)\approx(1/b)f(0)L=Nf(0)$, or formally as $\lim_{L\to 0} D_L(0)=Nf(0)$.

The quantities b and $L=Nb$ are dynamic variables of table/phantom motion (and intimately coupled thereby); therefore, artificially constraining one or both in Eqs. (2)–(4)

(such as fixing L in CTDI_{100}) will foil the convergence to $Nf(0)$ as $b\rightarrow 0$, and thus negate its relevance to SCBCT. Neither $Nf(z)$ nor $Nf(0)$ contain nT, which has no relevance in SCBCT dosimetry.

The following important points are clear from the foregoing:

(1) The integral of $f(z)$ over $(-L/2,L/2)$ for $D_L(0)$) in Eq. (3) and for CTDI_L in Eq. (4) *is solely the result of phantom translation* over the distance $L=vt_0=Nb$; moreover, the integration limits $\pm L/2$ and the divisor of the integral (the table increment $b=v\tau$) are necessarily coupled via $L=vt_0=Nb$ (coupled by couch velocity v for helical scans).
(2) The integral of $f(z)$ over $(-L/2,L/2)$ does not imply any averaging of the dose over the scan length L, but rather CTDI_L predicts the dose precisely at $z=0$ [at the center of the scan length $(-L/2, L/2)$] for helical scans at a pitch of unity.
(3) Physically, this integral represents a summation of the decreasing incremental contribution to the dose at $z=0$ by the scatter tails of the traveling profile as it gets further from the origin. And it is this lateral dispersal of the dose profiles due to phantom translation which results in the central dose at $z=0$ reaching a limiting equilibrium value D_{eq} for large scan lengths.
(4) CTDI always predicts the dose at (or about) the center of the scan interval $(-L/2,L/2)$ at $z=0$.
(5) For a stationary phantom ($v\rightarrow 0$, and $b=v\tau\rightarrow 0$, $L=vt_0\rightarrow 0$), and since the integration length $L\rightarrow 0$, the integral format of Eqs. (2)–(4) "collapses," smoothly converging in this limit to the nonintegral form $D_L(z)=Nf(z)$, or $D_L(0)=Nf(0)$, which increase without bound with N, since the individual dose profiles (deprived of lateral dispersal due to phantom translation) simply pile up on top of each other.

The properties (1)–(5) listed above also apply to axial scanning, which can be understood if one realizes that in this case, the integral over $(-L/2,L/2)$ in Eqs. (3) and (4) represents the smoothed version of the discrete summation $\tilde{D}_N(0)$ in Eq. (1).

In summary, for conventional CT scanning, CTDI_L [or any dose $D_L(0)=p^{-1}\mathrm{CTDI}_L$ derived from it] *always* represents the accumulated dose at (or about) the center of the scan length $(-L/2,L/2)$ at z=0. This also applies to MSAD,[4] $\mathrm{CTDI}_{\mathrm{w}}$ (Ref. 9), and $\mathrm{CTDI}_{\mathrm{vol}}$, the latter two are essentially planar averages over the *area* of the central scan plane at $z=0$, since no averaging over the scan length L has been performed.

II.B. The case of the stationary phantom

The dose distribution produced by a single axial rotation of a wide cone beam or a narrow fan beam having a primary beam width (FWHM)$=a$ (where a is also the projected z-collimator aperture setting) is denoted by $f(z)$ as before, and by $Nf(z)$ for N rotations without table translation, with a central ray peak dose $Nf(0)$.

Relating the dose and the dose distribution in SCBCT to that of conventional CT,

(1) The fact that CTDI_L represents the *dose* at the center $(z=0)$ of the scan length $(-L/2,L/2)$ in conventional CT suggests that its direct analog in the case of SCBCT would likewise be the dose $Nf(0)$ at the center $z=0$ of the beam $(-a/2,a/2)$ (on the "central ray" of the cone beam); corresponding to the location of the maximum or "peak" dose for both modalities.
(2) This conclusion is further supported by the physics which suggests that there should be little difference in the dose distribution $f(z)$ produced by a wide primary beam of width a (a cone beam) and the axial dose distribution $\tilde{D}_N(z)$ produced by a series of N adjacent, narrow primary beams of width $\hat{a}=a/N$, spaced at intervals $b=\hat{a}=a/N$, resulting in the same total energy deposition in the phantom as the cone beam, while "directly irradiating" (with the primary beam) the same length of phantom $L=Nb=a$.
(3) Using the beam model of Eq. (7) and $\tilde{D}_N(z)$ in Eq. (1), it is straightforward to show that the dose distribution $\tilde{D}_N(z)$ for the axial scan series described in (2) above for $b=\hat{a}=a/N$ and $L=a$ is equal to that for the cone beam of width a $[f(z)=\tilde{D}_N(z)]$; moreover, since $\tilde{D}_N(z)$ is smooth (since $b=\hat{a}$), the peak doses at $z=0$, $D_L(0)=\tilde{D}_N(0)=f(0)$ are all equal.
(4) This correspondence is directly confirmed using the experimental data of Mori *et al.*[1] from a 256 channel cone beam CT system for which dose profiles for all available cone beam widths (apertures) a ranging from 28 mm (rounded up from 27.5 mm), up to $a=138$ mm were measured. Figure 1 depicts the comparison described in (2) and (3) above in which the axial dose distribution $\tilde{D}_N(z)$ produced by the superposition (summation) of $N=5$ axial profiles of width $\hat{a}=28$ mm, spaced at like intervals $b=\hat{a}=28$ mm, where $L=Nb=140$ mm is seen to be coincident with the $a=138$ mm cone beam distribution $f(z)$ having $a=L$. ($L=5\times 27.5$ mm$=138$ mm exactly).
(5) This provides a direct physical connection between the dose $D_L(0)=p^{-1}\mathrm{CTDI}_L$ in conventional CT (described using CTDI_L) and the corresponding dose $f(0)$ in SCBCT, these doses being not only spatially colocated at $z=0$ but also equal in magnitude $D_L(0)\approx f(0)$, representing peak doses at $z=0$ in both cases as illustrated in Fig. 1.
(6) Therefore, $f(0)$ [or $Nf(0)$ for multiple rotations] is the obvious choice to represent the dose for stationary phantom CT for wide cone beams (SCBCT) and narrow fan beams alike. In fact, $f(0)$ is *the only choice* producing continuity between the two modalities. Use of any other "cone beam dose index" which predicted a dose other than $f(0)$ would amount to the paradoxical assignment of different "dose values" to the same dose distribution [i.e., for the same length of anatomy imaged using the same x-ray technique].

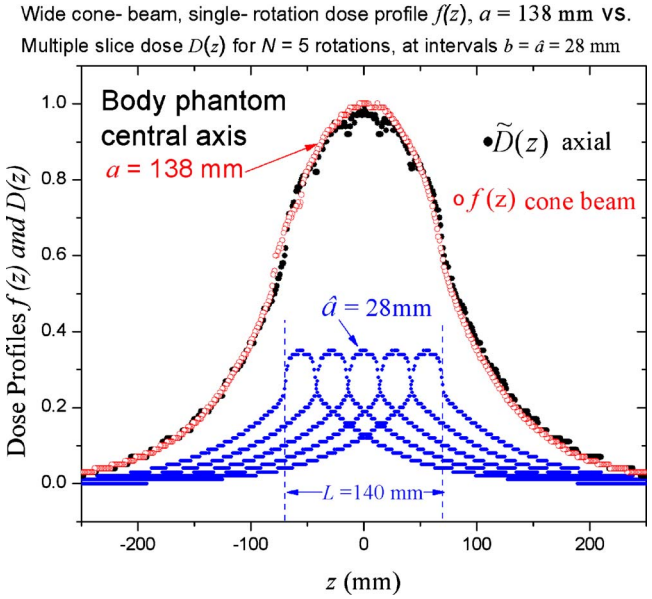

FIG. 1. The axial dose profile $f(z)$ for a wide cone beam of width $a=138$ mm generated by a single rotation about a stationary phantom (○) exhibits little difference from the accumulated dose distribution $\tilde{D}_N(z)$ (●) due to the superposition of $N=5$ axial profiles $\hat{f}(z)$ having $\hat{a}=28$ mm spaced at intervals (a table increment of) $b=\hat{a}=28$ mm, with a resulting a scan length $L=N\hat{a}=140$ mm; giving essentially the same directly irradiated length ($L=a$) as the cone beam having $a=138$ mm. The peak doses at $z=0$ are essentially equal, $\tilde{D}_N(0)\approx f(0)=1.0$, thereby corroborating the choice of $f(0)$ to represent the dose for SCBCT.

(7) It is also satisfying to note that the mathematics automatically forces the same conclusion, with the basic equations [Eqs. (1)–(4)], derived for conventional CT, all converging to the proper dose $Nf(z)$ for a stationary phantom in the limit as table advance $b\to 0$ as previously shown, thereby losing their integral format [including $\mathrm{CTDI}_L\to Nf(0)$, since $b=nT$ is a table advance and likewise this $b\to 0$].

II.B.1. Measurement of the central ray dose f(0) for a wide cone beam and a stationary phantom in SCBCT

- Since $f(0)$ is the dose on the central ray of the cone beam at depth in the phantom, the obvious (and simplest) method is to directly measure $f(0)$ at that point using a small ionization chamber (such as a 0.6 cc Farmer-type chamber), the same method used for decades to measure depth-dose in a stationary phantom.
- This same measurement method[2,3,10–12] has also been utilized in conventional CT to directly measure the accumulated dose $D_L(0)$ at $z=0$ during phantom translation over $(-L/2, L/2)$; its validity and robustness having been thoroughly demonstrated;[2] and which method also offers considerable advantages over the fixed-length pencil chamber, namely, unrestricted integration length (scan length) L, as well as broad applicability to shift-variant phantoms and techniques since it represents a direct dose measurement rather than a dose inferred from an integral acquired by irradiation of a pencil chamber.
- A pencil chamber *cannot* be used to measure $f(0)$ since it can only measure the integral of $f(z)$, and thus cannot distinguish between dose profiles having the same area but differing peak (or central ray) doses $f(0)$.

II.C. The equilibrium dose constant A_{eq}: A useful simplification obtained by setting the table advance b equal to the aperture a ($b=a$)

Returning to conventional CT scanning with phantom translation, an interesting and useful shortcut is described. Setting the scan interval $b=a$ (where a closely approximates the primary beam FWHM) produces scan contiguity in the dose domain. Since D_{eq} is proportional to (a/b), the equilibrium dose approached when $b=a$, denoted by $A_{eq}=(b/a)\,D_{eq}$ will depend on neither b nor a; and [using Eq. (5)] A_{eq} can be written as

$$A_{eq}=\frac{1}{a}\int_{-\infty}^{\infty} f(z')dz' = \text{constant}. \tag{6}$$

A_{eq} is a constant, independent of aperture a (and thence nT), since the integral is directly proportional to a as previously noted. For conventional CT, $D_{eq}=(a/b)A_{eq}$, thus A_{eq} is the equilibrium dose for a table advance $b=a$ (or a pitch $p=a/nT$).

The equilibrium dose constant $A_{eq}=(a/nT)^{-1}\mathrm{CTDI}_\infty$, although related to CTDI_∞, is not a proper CTDI, since $b=a$ represents a detector pitch $p=a/nT>1$ in MDCT for which a primary beam width $a>nT$ is required to keep the penumbra beyond the active detector length nT (referred to as "overbeaming") thus $A_{eq}<\mathrm{CTDI}_\infty$.

For conventional CT, overbeaming produces an increase in CTDI and accumulated dose by the factor a/nT (as compared to $a\approx nT$ for single slice scanners); however, overbeaming has less significance in SCBCT, producing a smaller dose increase since there are no overlapping, *adjacent* dose profiles.

Note that the aperture a corresponding to a given nT can be calculated from the dose efficiency, which is essentially equal to the inverse of the overbeaming factor $(a/nT)^{-1}$, and IEC standards[13] now require the dose efficiency to be supplied in the scanner technical documents (the dose efficiency may also be provided on the scanner monitor for some models). Typical apertures have also been published[2,5] for the GE Lightspeed family of scanners. However, as noted above, $(a/nT)^{-1}$ does not actually represent dose efficiency for stationary phantom CT (such as SCBCT). Use of A_{eq} allows a considerable reduction in data collection as will be illustrated, since its value can be fixed by making a measurement at single value of the aperture a.

TABLE I. Measured cone beam doses and dose integrals resulting from a single axial rotation about a stationary phantom (no table advance) for a 256 channel scanner (SCBCT) based on the data of Mori *et al.* (Ref. 1), where $f(z)$ denotes the axial dose profile corresponding to a primary beam width a on the central axis of the PMMA body phantom (32 cm diameter, 900 mm length), integrated over 900 mm to obtain the dose profile integral DPI_∞, all data being normalized per 100 mAs [measured data (Ref. 1)–central axis, body phantom].

Primary beam aperture a or FWHM (mm)	Dose profile integral $\mathrm{DPI}_\infty=\int_{-\infty}^{\infty}f(z)dz$	Equilibrium dose constant $A_{eq}=\mathrm{DPI}_\infty/a=1/a\int_{-\infty}^{\infty}f(z)dz$	Measured central ray dose $f(0)$	Ratio $A_{eq}/f(0)$
138 mm	848 mGy mm	6.14 mGy	4.37 mGy	1.43
111	686	6.18	3.90	1.58
80	498	6.22	3.19	1.95
49	303	6.18	2.27	2.72
28[a]	169	6.15	1.53	4.02

[a]Rounded off from 27.5 mm.

II.D. Numerical analysis of experimental SCBCT dose data

The experimental data of Mori *et al.*[1] obtained on a 256 channel cone beam CT scanner includes a direct measurement of both the central ray dose $f(0)$ as well as the infinite integral of the dose profile $f(z)$ denoted by DPI_∞; whose data can be used to illustrate the magnitude by which the actual dose $f(0)$ is overestimated should one attempt to apply CTDI_∞ to the problem (or by using CTDI_{300}, measured using a 300 mm long pencil chamber, to approximate CTDI_∞). As previously noted, nT has no relevance to the dose in stationary phantom CT (contiguity has no meaning and pitch $p=b/nT=0$).

The analysis is both simplified and made considerably more interesting if one uses A_{eq} from Eq. (6) as a "surrogate" for CTDI_∞, where $A_{eq}=(a/nT)^{-1}\mathrm{CTDI}_\infty<\mathrm{CTDI}_\infty$.

Table I illustrates the relationship between the measured central ray dose $f(0)$ and A_{eq} for various beam widths (aperture values) ranging from $a=28-138$ mm, resulting from a single axial rotation about the center ($z=0$) of a 900 mm long, 32 cm diameter, stationary PMMA body phantom.[1]

The original raw data[1] were reanalyzed to deduce the effective apertures a using the equivalent width[14] of the *primary beam* profiles as measured free-in-air[1] [$a\approx$width at $1/2f(0)$].

Thus the equilibrium dose constant $A_{eq}=(b/a)D_{eq}$ is indeed seen to be independent of aperture a as previously postulated, remaining constant to better than $\pm0.7\%$ over the entire range of apertures from $a=28-138$ mm; whereas $\mathrm{CTDI}_\infty=(a/nT)A_{eq}$ varies by a factor of 2.5 over the same range (corresponding nT values are 10, 32, 64, 96, and 128 mm); however, the important point is that A_{eq} significantly overestimates the relevant SCBCT dose $f(0)$ by the factor shown in the last column of Table I, viz., by a factor of 4 for a beam width of $a=28$ mm, by a factor of 2 for $a=80$ mm, and by a factor of 1.4 for $a=138$ mm, with CTDI_∞ giving an even larger overestimate (since $a>nT$). This result was previously anticipated since neither A_{eq} nor CTDI_∞ (described by integral equations) are relevant to the dose in stationary phantom CT (e.g., SCBCT).

The data in Table I are also illustrative of the magnitude of the error obtained in SCBCT when using a pencil chamber of length $\ell=300$ mm to measure CTDI_{300} (as an approximation to CTDI_∞) as illustrated by the following *Gedanken* experiment. Assume a cone beam width $a=115$ mm corresponding to $nT=100$ mm. By definition, CTDI_{300} is equal to the dose at the center of *three contiguous* axial scans, each with $nT=100$ mm, stitched together using an interval (a table advance) of $b=nT=100$ mm, for a total scan length of $L=Nb=300$ mm. In this case CTDI_{300} overestimates the SCBCT peak dose $f(0)$ by about 60%, due to scatter from the two additional contiguous scans which augment the dose $f(0)$ at $z=0$ [$\mathrm{CTDI}_{300}=1.6f(0)$].

The notion that the integral equations for CTDI_∞ or A_{eq} might predict some useful average dose for SCBCT is readily dispelled; since it is clear from the data in Table I and Fig. 1, that A_{eq} and thus CTDI_∞ (and CTDI_{300}) are both larger than the peak dose $f(0)$ for every available aperture setting, i.e., their associated dose values do not exist anywhere in the phantom. Mathematically, in order to obtain $f(0)$ from $\int_{-\infty}^{\infty}f(z)dz$, one must divide the integral by the equivalent width[14] a_w of the function; however, since $f(z)$ contains a broad scatter component, a_w is larger than the *primary beam width* a (or nT) used as divisors in computing A_{eq} (or CTDI_∞) [e.g., for the $a=28$ mm profiles shown in Fig. 1, $a_w=112$ mm, for which A_{eq} overestimates $f(0)$ by a factor of $(a_w/a)=4$.]. Thus A_{eq} (or CTDI_∞) will always overestimate $f(0)$. So why do we divide the integral by the primary beam width? We do not—These divisors represent *table increments* $b=a$ for A_{eq} (or $b=nT$ for CTDI) and not primary beam widths (actual or nominal). The CTDI paradigm was never intended to predict the dose $f(0)$ for a single axial rotation, but rather the accumulated dose $D_L(0)$ at $z=0$ for N multiple scans, spaced at intervals b due to table translation over a length $L=Nb$.

A small ion chamber can precisely measure the desired peak dose $f(0)=1.0$ in Fig. 1, whereas the "dose" values given by the "CTDI types" are $A_{eq}=1.4$, $\mathrm{CTDI}_\infty=1.5$, and $\mathrm{CTDI}_{300}=1.4$, all lying well above the peak dose $f(0)=1.0$ (even above the top of Fig. 1).

Since A_{eq} is independent of aperture a, a narrow beam can be used to measure A_{eq} if the aperture a is known; however, this is small consolation since the values of both A_{eq} and CTDI_∞ overestimate the dose $f(0)$ in SCBCT for clinically relevant cone beam widths (see Table I). The SCBCT dose $f(0)$ would exhibit a variation of more than 200% (a factor of

2.3) over the range of beam widths $a=50-180$ mm available for clinical use on the aforementioned 320 channel SCBCT scanner (corresponding to $nT=40-160$ mm); and a much larger variation in the case of narrow fan beams also used in stationary phantom CT such as in CT fluoroscopy or perfusion studies [for which the peak dose $f(0)$ may be significantly overestimated[15] by attempting to apply the dose paradigm based on CTDI_{100} [we note that the IEC definition[13] of $\mathrm{CTDI}_{\mathrm{vol}}$ utilizes $N\times\mathrm{CTDI}_{100}$ compared to the actual dose $Nf(0)$].

It is therefore important to determine $f(0)$ over the complete range of apertures used clinically in the SCBCT acquisition mode, e.g., for ($40\ \mathrm{mm}\leq nT\leq 160\ \mathrm{mm}$). A useful theoretical function is derived in Sec. III describing the variation in $f(0)$ with a, which closely matches the data in Table I; and which can be used to extrapolate a measurement of $f(0)$ at a single value of aperture a to any other aperture; thus allowing the prediction of the peak doses $f(0)$ for narrow fan beams which would require an ion chamber length $\ell<nT$ for the central axis measurement.

II.D.1. The approach to scatter equilibrium

From the data in Table I, it appears that $f(0)$ is increasing *toward* A_{eq} as the cone beam width a increases, and such a convergence does indeed occur, but only for very wide (and thus clinically irrelevant) cone beam widths of $a\geq 470$ mm. Like the accumulated dose $D_L(0)$ in conventional CT, the SCBCT dose $f(0)$ will also asymptotically approach a maximum equilibrium value $f_{\mathrm{eq}}(0)$ when the cone beam width a becomes wide enough to achieve scatter equilibrium on the central ray at $z=0$, such that scatter produced from any further increases in primary beam width can no longer reach $z=0$, and thus no longer affect $f(0)$. Attainment of equilibrium at $z=0$ depends only on the *distance* of the outermost primary beam photons from the origin. When the probability becomes negligible that primary photons scattered at the far-flung primary beam edges (at $z'=\pm a/2$ for the cone beam or at $z'=\pm L/2$ in conventional CT) can reach the origin, then equilibrium is achieved for cone beam widths $a\geq a_{\mathrm{eq}}$, and likewise for scan lengths $L\geq L_{\mathrm{eq}}$ for conventional CT, thus it follows that $a_{\mathrm{eq}}=L_{\mathrm{eq}}$. Likewise, the magnitude of the equilibrium dose constant A_{eq} is the same for both modalities. (These results follow from our previous arguments demonstrating the equality of the dose at $z=0$ for the two modalities for the case $L=a$.)

Since $L_{\mathrm{eq}}\approx 470$ mm in conventional CT,[16] scatter equilibrium at $z=0$ will therefore occur for cone beam widths $a\geq 470$ mm in the 32 cm PMMA body phantom. However, since such wide cone beams are not utilized (nor likely to be) in this modality, the cone beam equilibrium dose $f_{\mathrm{eq}}(0)=A_{\mathrm{eq}}$ is not clinically relevant for SCBCT; whereas, for conventional CT scanning, typical body scan lengths of $L\geq 250$ mm produce doses which closely approach D_{eq}; therefore D_{eq} or CTDI_{∞} [and likewise $A_{\mathrm{eq}}=(b/a)\ D_{\mathrm{eq}}$)] is a considerably more relevant dose for this modality. However, the value of A_{eq} can serve as a convenient, common normalization constant for both modalities.

II.D.2. The approach to equilibrium function $H(\lambda)$

The variation in the relative approach to equilibrium function $H(a)=[f(0)/f_{\mathrm{eq}}(0)]$ is conceptually quite similar to the increase in dose at a given depth with increasing field size observed for a stationary x-ray beam incident on a phantom (except only one field dimension a is varied in this case). In fact, the SCBCT equilibrium dose is the same as A_{eq} for conventional CT, viz. $f_{\mathrm{eq}}(0)=A_{\mathrm{eq}}$; and the relative approach to equilibrium curves $H(L)=D_L(0)/D_{\mathrm{eq}}$ and $H(a)=f(0)/A_{\mathrm{eq}}$ should be the same using the correspondence $a=L$, based on our previous analogy between a cone beam and a juxtaposition of adjacent narrow fan beams.

III. MODELING THE CONE BEAM

For definiteness and simplicity, all numerical examples and derivations refer to the dose on the central axis of the 32 cm diameter cylindrical PMMA body phantom at 120 kVp using a bow-tie filter unless otherwise noted. The peripheral axis is dealt with in Sec. IV.

III.A. General considerations

As previously seen in Fig. 1, there is nothing particularly mysterious about the SCBCT axial dose profile $f(z)$ for a wide cone beam of width a, being quite similar to the cumulative dose distribution $D_L(z)$ in conventional CT at a pitch near unity ($p=\hat{a}/nT$) for the same directly irradiated phantom length $L=a$. Differences in beam divergence between the narrow beams and wide cone beam are quite small (only about $\pm 7°$ deg from the central ray at the extreme edges $z=\pm a/2$ of the widest cone beam, $a=138$ mm).

III.A.1. The heel effect

The only real difference is that the wider collimator aperture of the cone beam enhances the heel effect; however, neither its odd nor its even components[5] have any significant effect on the central ray dose $f(0)$ [the SCBCT dose-descriptor of interest], with both the primary and the scatter components at $z=0$ being essentially unaffected. Thus, a simple model which ignores anode tilt and the heel effect should do quite nicely for predicting the relevant SCBCT dose $f(0)$, but may do somewhat less well in reproducing the entire dose distribution $f(z)$, particularly near the beam edges for wide cone beams on the peripheral axes. It also produces the same results as a more complex model[5] (including anode tilt and the heel effect) for the integral theorems involving A_{eq} and D_{eq}.

III.B. A simple beam model predicting the observed dose data

The *primary beam* LSF is the focal spot emission intensity[5] (as slit-projected by the z-collimators onto the AOR), and expressed as a scaled function $\mathrm{lsf}(z)=c^{-1}g(-z/c)$ having unit area, where c represents the slit-projected focal spot length ($c\sim 3$ mm).

The *scatter* LSF $(z-z')$ is the much broader scatter response function to a unit-strength primary beam impulse

$\delta(z')$ (or "knife edge") applied at $z=z'$, where η is the scatter to primary ratio S/P, where η is equal to the ratio of scattered to primary energy deposited along z as expressed by the ratio $\eta=S/P$, where $S=\int_{-\infty}^{\infty}f_s(z')dz'$ and $P=\int_{-\infty}^{\infty}f_p(z')dz'$. Thus $\int_{-\infty}^{\infty}\mathrm{LSF}(z)dz=\eta$, and it is convenient to express $\mathrm{LSF}(z)=\eta\,\mathrm{lsf}(z)$ where $\mathrm{lsf}(z)$ is a unit-area scaled function, symbolically represented as $\mathrm{lsf}(z)=d^{-1}h(z/d)$, where d represents the width of the broad scatter LSF ($d\sim 100$ mm) and where $d\gg c$.

The model generates the primary beam component $f_p(z)$ and the scatter component $f_s(z)$ of the axial dose profile $f(z)=f_p(z)+f_s(z)$ by the convolution shown below

$$f(z)=\left[\frac{1}{c}g\left(\frac{-z}{c}\right)+\eta\frac{1}{d}h\left(\frac{z}{d}\right)\right]\otimes A_0\Pi\left(\frac{z}{a}\right), \tag{7}$$

where $A_0\Pi(z/a)$ represents the core primary beam function (without penumbra). The convolution of the focal spot $\mathrm{lsf}[c^{-1}g(-z/c)]$ with $A_0\Pi(z/a)$ produces the primary beam function $f_p(z)$ by adding a penumbra of width c to $\Pi(z/a)$, and the convolution of the scatter $\mathrm{LSF}(z)=\eta\,\mathrm{lsf}(z)=\eta d^{-1}h(z/d)$ with the primary beam core $A_0\Pi(z/a)$ gives the scatter component $f_s(z)$, where the negligible effect of the primary beam penumbra on the scatter distribution has been ignored (its effect is truly nil).

Since in MDCT the penumbra c is necessarily small compared to the aperture setting a, the width c of the penumbra added to $\Pi(z/a)$ by its convolution with $c^{-1}g(-z/c)$ is small compared to a ($c\ll a$), in which case $A_0=f_p(0)$ which is the "point dose" on the central ray ($z=0$) contributed by the primary beam at isocenter (at a depth of 16 cm in the body phantom) [as the aperture a is decreased to a value comparable to the penumbra c, the beam FWHM actually increases, becoming larger than a and its peak intensity $f_p(0)$ decreases below the emitted intensity A_0 due to narrow slit effects[5]. This effect required postpatient collimation to achieve narrow slice widths for single slice scanners].

III.B.1. The integral theorem

The expression for the infinite integral of $f(z)$, and thence the equilibrium dose constant A_{eq} in Eq. (6) (or CTDI_∞), immediately follows from Eq. (7) without requiring any detailed knowledge of the functional form of $f(z)$ (or that of either lsf); the infinite integral of the convolution in Eq. (7) being obtained by inspection as

$$\int_{-\infty}^{\infty}f(z')dz'=A_0(1+\eta)a=f_p(0)(1+\eta)a, \tag{8}$$

which shows the important proportionality of the infinite integral of $f(z)$ to the aperture a, and also providing the theoretical formula for A_{eq} shown below

$$A_{\mathrm{eq}}=\frac{1}{a}\int_{-\infty}^{\infty}f(z')dz'=A_0(1+\eta)=f_p(0)(1+\eta), \tag{9}$$

thereby confirming the constancy of A_{eq}, namely, its independence of aperture setting a (and also of nT). Equation (9) shows that A_{eq} depends only on the primary beam intensity $f_p(0)$ on the central ray, which is well-known to be independent of collimator setting (assuming $a>c$), and on the S/P ratio η (since η is also the impulse-response amplitude, it cannot depend on a); and also confirms that A_{eq} is the same for conventional CT and SCBCT.

The equilibrium dose for conventional CT can be written as $D_{\mathrm{eq}}=(a/b)\,A_{\mathrm{eq}}$, which is directly proportional to (a/b) since A_{eq} is a constant (physically, opening the collimator aperture a deposits more energy per rotation, and reducing b packs the dose profiles into a smaller length, both leading to an increase in dose). Thus D_{eq} for conventional CT can have different values, depending on both the aperture a (and thence nT) and the table increment b (or helical pitch $p=b/nT$), and $D_{\mathrm{eq}}=A_{\mathrm{eq}}$ only for a table advance of $b=a$; however, for SCBCT the scatter equilibrium limit for the dose $f(0)$ is always A_{eq} (a constant).

The constancy of A_{eq} predicted by this model remains valid even for wide cone beams, as clearly illustrated by the experimental data in Table I. This broad general result follows physically from the conservation of energy, the total amount of energy escaping the collimator, impinging on the phantom, and absorbed in the phantom is directly proportional to the aperture a which acts as an energy gate; thus the constancy of A_{eq} holds along any phantom axis, central or peripheral. Note also that the infinite integrals of the primary beam and scatter components are both (separately) proportional to aperture a, thus a free-in-air measurement[2] of CTDI_∞ (air) is proportional to a and thus can provide the relative variation of aperture a with nT.

III.B.2. Relation between A_{eq} and the total energy deposited in the phantom (integral dose)

For an axial or helical scan series, the total energy E deposited (absorbed) in the phantom along a given z-axis is represented by the infinite integral of $\tilde{D}(z)$ in Eq. (1), or of $D_L(z)$ Eq. (2), either resulting in $E=N\int_{-\infty}^{\infty}f(z)dz=NA_{\mathrm{eq}}a$; the same formula as for the total energy deposited by N rotations about a stationary phantom (as for SCBCT) for which the dose distribution is $Nf(z)$. With good reason, the total energy deposited by N rotations is independent of their spread or distribution along z and depends (for a given kVp and bowtie filter) only on the product of $N\times$(mAs per rotation) $\times$(aperture a), or simply on the product of (total mAs) $\times$(aperture a); and the total energy E deposited is the same whether the table moves or not (which likewise applies to the DLP[9]).

III.B.3. Calculation of the relevant stationary phantom peak dose $f(0)$ using this model

To obtain the desired dose $f(0)$, we evaluate $f(z)$ in Eq. (7) at $z=0$, which is a simple task for the primary beam intensity A_0 which is given by $f_p(0)=A_0$ for the case where $a>c$; however, for the scatter component, neither d nor a dominate sufficiently, and the convolution gives a scatter component of

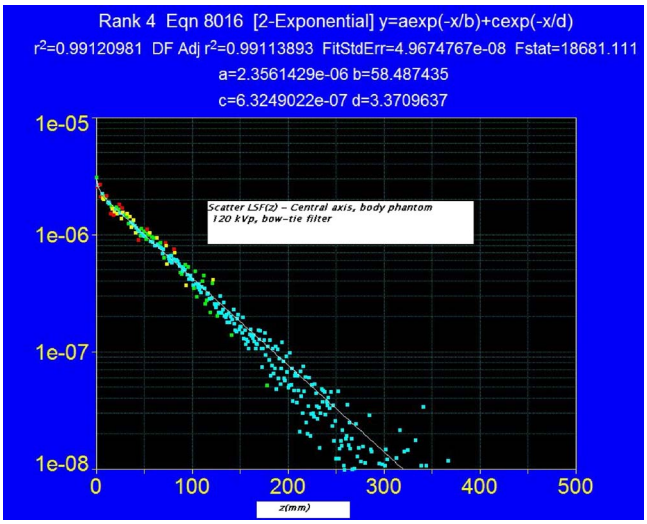

FIG. 2. Scatter LSF, central axis 32 cm diameter PMMA body phantom with double-exponential fit function (arbitrary units). Data from a Monte Carlo simulation (Ref. 17) at 120 kVp with a body bow-tie filter.

$$f_s(z) = A_0\eta\int_{-\infty}^{\infty} d^{-1}h\left(\frac{z-z'}{d}\right)\Pi\left(\frac{z'}{a}\right)dz'$$

$$= A_0\eta\int_{-a/2}^{a/2} d^{-1}h\left(\frac{z-z'}{d}\right)dz'. \quad (10)$$

Since our goal is to determine the central ray dose $f(0)$ in the stationary phantom which is used as the dose-descriptor for SCBCT, setting $z=0$ in Eq. (10) to obtain $f_s(0)$ and adding the primary beam component $f_p(0)=A_0$ to the scatter component, $f(0)=f_p(0)+f_s(0)$, the total central ray dose is given by

$$f(0) = f_p(0)\left[1+\eta\frac{1}{d}\int_{-a/2}^{a/2} h\left(\frac{z}{d}\right)dz\right]. \quad (11)$$

If $a \gg d$, the above integral is essentially infinite, and $f(0)=f_p(0)(1+\eta)=A_{eq}$, corresponding to scatter equilibrium being attained at $z=0$.

III.B.4. The scatter LSFs exhibit surprising simplicity

Further results from this model require a more detailed knowledge of the scatter LSF$(z)=\eta$lsf(z) on the phantom axis. To that end, Boone[17] has recently performed Monte Carlo (MC) dose simulations in a variety of cylindrical phantoms (with and without bowtie filters); and more importantly has provided the data in their most useful and concise form, namely, as a scatter LSF which can be used as a "kernel" in the integral expressions derived above to calculate $f(0)$ [as well as $f(z)$] for any beam width a, without requiring any additional MC simulations. Moreover, these scatter LSFs exhibit a surprising simplicity, asymptotically approaching a pure, single-exponential of the form $\exp(-\mu_r z)$ a few cm beyond $z=0$, thus allowing the theoretical results to be expressed as simple analytical functions.

Figure 2 shows the scatter LSF(z) obtained by Boone[17] for the central axis of a 32 cm diameter PMMA phantom of infinite length at 120 kVp with bow-tie filter, this function being readily fit by a double-exponential decay as shown. Only half of the even function LSF(z)=LSF$(-z)$ is shown.

Renormalizing the scatter LSF function fit parameters shown in Fig. 2 to conform to our notation (using scaled, unit-area lsf functions), where LSF$=\eta\times$lsf(z), it becomes

$$\text{lsf}(z) = (1-\varepsilon)\frac{1}{d}\exp(-2|z|/d) + \varepsilon\frac{1}{\delta d}\exp(-2|z|/\delta d), \quad (12)$$

where $d=117$ mm, $\delta d=6.74$ mm$=.0576d$, and where $(1-\varepsilon)=0.985$ and $\varepsilon=0.015$ are the respective *areas* of the asymptotic first term, and the transient second term; and where the S/P ratio[17] is $\eta=13$ for the central axis of the body phantom. The transient second term in Eq. (12) becomes negligible for $z>10$ mm, after which the lsf reaches its single-exponential asymptotic form, which when written as $\exp(-\mu_r z)$, corresponds to a value of $\mu_r=0.17$ cm^{-1}.

The transient second term in Eq. (12) produces little effect for cone beams (or beams having widths $a>20$ mm), and the lsf can be approximated quite well in this case by the first term of Eq. (12) as a single-exponential (renormalized to unit area), namely, as

$$\text{lsf}(z) = d^{-1}h(z/d) \cong d^{-1}\exp(-2|z|/d) \quad (13)$$

in which $d=117$ mm.

III.B.5. Derivation of the equation for the peak dose f(0) using the scatter LSF

Substitution of the simplified Eq. (13) into Eq. (11) and integrating yields

$$f(0) \cong f_p(0)[1+\eta(1-e^{-a/d})]. \quad (14)$$

Using the more accurate double-exponential fit to the lsf given *by* Eq. (12), which is more appropriate (more accurate) for narrow fan beams, gives

$$f(0) = f_p(0)\{1+\eta[(1-\varepsilon)(1-e^{-a/d})+\varepsilon(1-e^{-a/\delta d})]\}. \quad (15)$$

Both Eqs. (14) and (15) approach the same limiting dose value for $a \gg d$, $f(0)\to f_p(0)[1+\eta]=A_{eq}$, and for all practical purposes (within 2%) when $a \geq a_{eq}=4d=470$ mm [from $e^{-a/d}=e^{-4}=0.018$ in Eqs. (14) and (15)]. Although this expression for $A_{eq}=f_p(0)[1+\eta]$ was previously obtained in Eq. (8) using the convolution integral theorem, this model provides a clear physical insight and a functional form (an exponential growth function) describing the approach of $f(0)$ toward its (unattainable) equilibrium value A_{eq}, clearly illustrating that this occurs only in the limit where the cone beam width a itself becomes large with respect to the width $d=117$ mm of the scatter LSF, namely, for $a \geq 4d=470$ mm. For a primary beam width $a=4d$, a primary photon scattered at the extreme edges of the beam $z=\pm a/2$ has only a negligible chance of getting back to $z=0$ to contribute to the center dose $f(0)$ [a survival probability of $\exp(-\mu_r a/2)=e^{-4}$]. The same LSF and thus the same argu-

ment applies to conventional CT; a primary photon scattered from the extremes of the scan length at $z=\pm L/2$ where $L=4d$ has exactly the same chance (e^{-4}) of making it back to $z=0$ to contribute to $D_L(0)$; therefore, the equilibrium lengths are identical for the two modalities, i.e., $L_{eq}=a_{eq}=4d=470$ mm on the central axis.

Although A_{eq} (like CTDI) does not represent a meaningful or relevant dose value for SCBCT, it has utility as a convenient normalization constant for the common approach to equilibrium function $H(\lambda)$, which becomes $H(L)$ for conventional CT and $H(a)$ in stationary phantom CT.

III.B.6. The approach to equilibrium function H(a)

The relative "approach-to-equilibrium" function $H(a)=f(0)/A_{eq}$ for the stationary phantom using the more general Eq. (15) is given by

$$H(a)=\frac{1}{1+\eta}+\frac{\eta}{1+\eta}[(1-\varepsilon)(1-e^{-a/d})+\varepsilon(1-e^{-a/\delta d})]. \tag{16}$$

The first term $1/(1+\eta)$ represents the relative primary beam contribution and the second term the relative scatter contribution; however, since $\delta d=6.74$ mm, the transient scatter term grows very quickly to its small limiting value $\varepsilon=0.015$ for $a>25$ mm, representing only 1.5% of the total scatter at equilibrium.

A simplified form of $H(a)$ applicable to the wider beams of SCBCT is obtained using the single-exponential scatter lsf in Eq. (13) which produces $f(0)$ in Eq. (14), and which in turn gives.

$$H(a)\cong\frac{1}{1+\eta}+\frac{\eta}{1+\eta}(1-e^{-a/d}). \tag{17}$$

The second term in both equations represents the scatter contribution which has the form of an exponential growth curve, increasing with beam width a until reaching its asymptotic (equilibrium) limit $H(a)\to 1$ for $a\geq 4d\approx 470$ mm, the fractional scatter contribution at equilibrium being $\eta/(1+\eta)$ and the relative primary contribution $1/(1+\eta)$.

III.B.7. The commonality of the approach to equilibrium function H(a) for both stationary phantom scanning (e.g., SCBCT) and conventional CT scanning

Note that the same scatter LSF function applies both to stationary beam CT and conventional axial or helical CT [usable in both cases to create an axial dose profile $f(z)$ in Eq. (7)]; however, this profile must additionally be integrated over $(-L/2,L/2)$ for conventional CT to obtain the accumulated dose $D_L(0)$ at $z=0$ [Eq. (3)] or $CTDI_L$ [Eq. (4)], resulting in the additional dependence of the equilibrium dose D_{eq} in conventional CT on the table increment b (or pitch $p=b/nT$) and aperture a, i.e., $D_{eq}=(a/b)A_{eq}$ is proportional to (a/b) as noted previously. The integral theorem [Eq. (9)] shows that the equilibrium dose constant $A_{eq}=(b/a)D_{eq}=f_p(0)(1+\eta)$ has the same value for both SCBCT and conventional CT, being independent of aperture a (and scan length L).

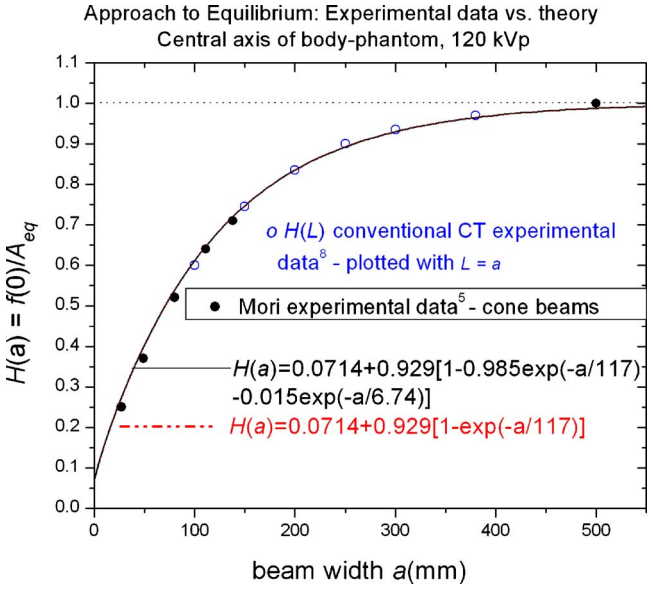

FIG. 3. Approach to scatter equilibrium theory vs experiment. Relative approach to equilibrium function $H(a)=f(0)/f_{eq}(0)=f(0)/A_{eq}$ on the central axis of a stationary phantom (e.g., SCBCT). The solid circles (●) are the experimental data of Mori[1] presented in Table I. The solid and dashed lines representing $H(a)$ *are not empirical fits* but rather theoretical predictions obtained from the mathematical model; the solid black line representing the full double-exponential scatter lsf Eq. (16), and the essentially congruent dotted-dashed line using the simpler single-exponential approximation of the scatter lsf Eq. (17). Also plotted is the experimental approach to equilibrium data for conventional CT scans measured[2] on GE 16 channel and 64 channel scanners for scan lengths L from 100 to 400 mm, and plotted (○) using the correspondence $L=a$; thus validating the same functional form for both modalities, $H(L)=H(a)$ with the correspondence $a=L$.

The cone beam dose $f(0)$ necessarily approaches the same equilibrium dose value $f_{eq}(0)=A_{eq}$ with increasing aperture setting a (although it will never get there for practical cone beam widths).

Comparing SCBCT with aperture a to conventional CT with N rotations of aperture $\hat{a}=a/N$ and $b=\hat{a}$ for which $L=Nb=a$, it was previously shown (and observed in Fig. 1) that $D_L(0)=f(0)$. Therefore, since $f(0)_a=D_L(0)$ for $L=a$, then $H(L)A_{eq}=H(a)A_{eq}$, thus $H(L)=H(a)$ for $L=a$; hence a common function $H(\lambda)$ applies to both modalities with $\lambda=L$ or $\lambda=a$.

The function $H(L)$ is essentially independent of aperture,[5,16] since both D_{eq} and $D_L(0)$ are proportional to $\hat{a}$ [rigorously in the case of D_{eq} and approximately[5] for $D_L(0)$] at least over an aperture range corresponding to (2.5 mm $\leq nT\leq$ 40 mm). Boone[16] has shown that $H(100\text{ mm})=[CTDI_{100}/CTDI_\infty]=[D_{100}(0)/D_{eq}]$ varies by less than 1% over this range of apertures.

III.B.8. Comparison of the theoretical equation for H(a) with experiment

Does our *mathematical model of the dose profile* $f(z)$, correctly predict the measured[1] variation in $f(0)$ with aper-

TABLE II. Mori (Ref. 1) data for the peripheral axis of the body phantom.

Primary beam aperture a or FWHM (mm)	Dose profile integral $\mathrm{DPI}_\infty=\int_{-\infty}^{\infty}f(z)dz$	Equilibrium dose constant $A_{eq}=\mathrm{DPI}_\infty/a=1/a\int_{-\infty}^{\infty}f(z)dz$	Measured central ray dose $f(0)$	Ratio $A_{eq}/f(0)$
138 mm	1520 mGy mm	11.0 mGy	9.60 mGy	1.14
111	1220	11.0	9.02	1.21
80	900	11.1	8.54	1.28
49	530	10.6	8.06	1.35
28[a]	290	10.6	7.34	1.49

[a]Rounded off from 27.5 mm.

ture a given in Table I? Or equivalently, does the derived analytic function $H(a)=f(0)/A_{eq}$ given by Eq. (16) [or approximated by Eq. (17) for cone beams] agree with the observed ratio computed from the experimental data[1] in Table I? Figure 3 answers this affirmatively illustrating the excellent agreement between the theoretical predictions of Eqs. (16) and (17) (the curves) and the experimental values[1] of the relative, stationary phantom peak doses $f(0)_a$ shown by the solid data points (•)*It should be emphasized that this is not empirical curve fitting*, but rather comparing a physical theory having no adjustable parameters as embodied by Eq. (16) to the observed experimental data, thereby giving added confidence in its general applicability.

The single-exponential approximation of the lsf in Eq. (13) leading to the simple growth curve $H(a)$ of Eq. (17) is indistinguishable from the double-exponential form of the lsf which produces $H(a)$ in Eq. (16) also shown in Fig. 3.

The premise that the same function $H(a)$ can also predict the variation in the accumulated dose $D_L(0)$ at $z=0$ with scan length L for conventional CT simply by making the substitution $L=a$ in Eq. (17) is also confirmed by plotting experimental values[2] of $H(L)$ measured using helical scans on 16 and 64 channel GE scanners (open circles in Fig. 3), which data also fall on the theoretical curves, thereby confirming this premise, at least over the measurement range used ($100\ \mathrm{mm}\leq L\leq 400\ \mathrm{mm}$). It should be noted, however, that $H(L)$ refers to the variation in dose in a phantom *at least* 500 mm long, and cannot be used without correction to extrapolate CTDI_{100} measured in a standard 140 mm long body phantom to predict CTDI_∞, or $D_{eq}=p^{-1}\mathrm{CTDI}_\infty$ (e.g., an increase in body phantom length from 150 to 400 mm was observed[2] to produce an increase in the measured value of CTDI_{100} by 7.3% on the central axis and by 1.3% on the peripheral axis at 120 kVp).

III.C. Extension to peripheral axes

Due to the potential practical utility of the derived analytical functions, it behooves us to make a similar (but abbreviated) analysis for the peripheral axis of the same body phantom (a more complex problem).

That A_{eq} as defined in Eq. (6) is likewise a constant (independent of aperture a) on the peripheral axis is confirmed using the experimental data of Mori[1] as shown in Table II.

The normalized (to unit area) lsfs for the central and peripheral axes are both shown in Fig. 4 for comparison. The double-exponential fit proved reasonably successful for the peripheral axis, resulting in the lsf fit parameters of $\varepsilon=0.304$, $\delta d=14$ mm, and $d=88$ mm which, together with $\eta=1.5$, give a scatter LSF as described by Eq. (12).

III.C.1. Derivation of the expression for f(z) and f(0) on the peripheral axis using the LSF

As discussed previously,[5] the convolution model [Eq. (7)] strictly holds only for a fixed gantry angle θ on a peripheral axis, since the parameters η, a, c, the lsf, and $A_0=f_p(0)$ are all functions of beam angle θ; thus Eq. (7) must be written as $f(z,\theta)$ and then averaged (integrated) over 2π in order to obtain the axial dose profile $f(z)$ on the peripheral axis, thereby losing the convolution format for $f(z)$ and possibly the applicability of the LSF (also mentioned by Boone[17]). However, as shown in Appendix A, if $\theta=0$ denotes the gantry angle for which the beam is directly incident on the peripheral axis in question, then most of the dose on that axis is delivered for a small enough angular range $\pm\Delta\theta$ about $\theta=0$, such that $a(\theta)$ is slowly varying over $\pm\Delta\theta$ and can be replaced by its average value $\langle a\rangle$, which is the FWHM of the

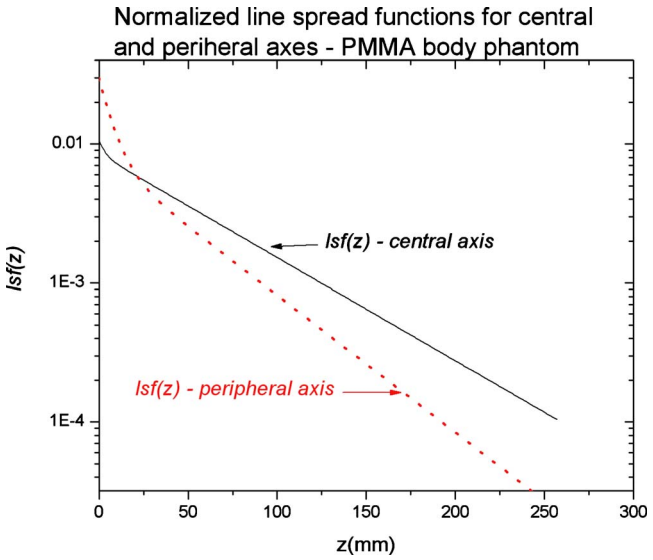

FIG. 4. Scatter lsf for the central and peripheral axes in a 32 cm diameter PMMA phantom normalized to unit area. The actual LSF=$\eta\times$lsf, where $\eta=S/P$ ratio with $\eta=13$ for the central axis and $\eta=1.5$ for the peripheral axis (Ref. 17); thus the absolute peripheral axis LSF falls below that for the central axis as expected.

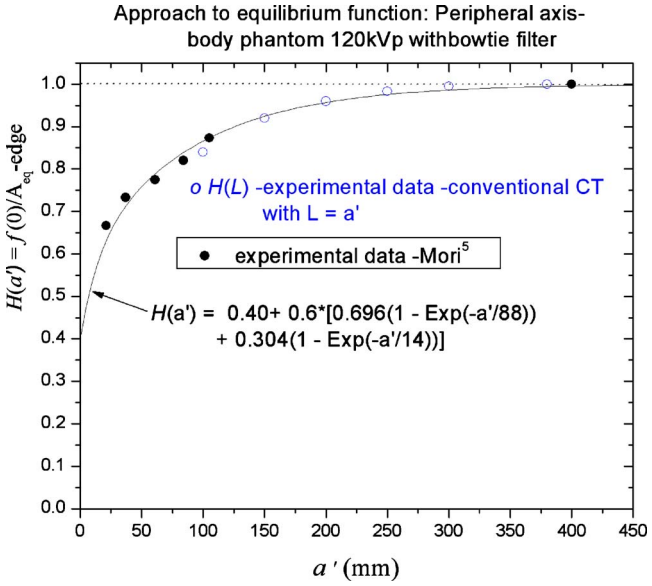

FIG. 5. Approach to equilibrium function $H(a')$ on the peripheral (edge) axis of the body phantom plotted vs the FWHM a' of the cone beam dose profile $f(z)$ on that axis, together with the experimental data of Mori (Ref. 1) and helical scan data (Ref. 2) plotted using $L=a'$.

axial dose profile $a'=\langle a\rangle$ on the peripheral axis [and which is only about 5% greater[5] than the minimum value of $a(\theta)$ at $\theta=0$]. Thus Eq. (15) for $f(0)$ and Eq. (16) for $H(a)$ also apply, with a replaced by a', and using the corresponding peripheral axis (double-exponential) fit parameters $\varepsilon=0.304$, $d=88$ mm, and $\delta d=14$ mm, and a S/P ratio of $\eta=1.5$.

$$H(a')=\frac{1}{1+\eta}+\frac{\eta}{1+\eta}\times[(1-\varepsilon)(1-e^{-a'/88\ \mathrm{mm}})+\varepsilon(1-e^{-a'/14\ \mathrm{mm}})]. \tag{18}$$

The parameter a', the FWHM of the peripheral axis profile $f(z)$ which automatically appears in the peripheral axis equations for $f(0)$ and in $H(a)$, is the physically significant parameter *for comparing modalities* on the peripheral axis, i.e., an axial scan series using beams of width a'/N at a like scan interval $b=a'/N$ with $L=Nb=a'$ will produce a relatively smooth dose distribution (without gaps) on the peripheral axis which is comparable to a cone beam distribution $f(z)$ of width a'. Figure 5 shows the relative stationary phantom, peripheral axis peak dose experimental data[1] in Table II plotted vs $a'=0.76a$ compared to the theoretical curve $H(a')$ in Eq. (18). Likewise, the experimental conventional peripheral axis CT data[2] $H(L)$ is plotted using the correspondence $L=a'$, with both data sets exhibiting reasonably good agreement between experiment and the theoretical curve $H(a')$ in Eq. (18).

Since a' is proportional to the central axis aperture projection a, either could be used to evaluate A_{eq} as noted in Appendix A (it is independent of aperture), and it is more convenient to work with a and $H(a)$ as was done in Table II. By substituting $a=a'/0.76$ into $H(a')$ we obtain

$$H(a)=\frac{1}{1+\eta}+\frac{\eta}{1+\eta}\times[(1-\varepsilon)(1-e^{-a/116})+\varepsilon(1-e^{-a/18.4})], \tag{19}$$

where now $d=88/0.76=116$ mm, $\delta d=14/0.76=18.4$ mm, with $\varepsilon=0.305$ and $\eta=1.5$ as before. (It is interesting that $d=116$ mm which determines asymptotic equilibrium is essentially the same as on the central axis where $d=117$ mm.) Of course, $H(a)$ in Eq. (19) is completely equivalent to $H(a')$ in Eq. (18) in which $d=88$ mm and $\delta d=14$ mm.

For comparison with conventional CT we must still substitute $L=a'$ into $H(a')$ in order to obtain

$$H(L)=\frac{1}{1+\eta}+\frac{\eta}{1+\eta}[(1-\varepsilon)(1-e^{-L/88})+\varepsilon(1-e^{-L/14})], \tag{20}$$

where $H(L)=D_L(0)/D_{\mathrm{eq}}$ and $D_{\mathrm{eq}}=(a/b)A_{\mathrm{eq}}$.

The reason Eqs. (18) and (19) differ in form but not substance is that the scan length L does not diverge (it is the same for the central and peripheral axes), whereas the beam width a does diverge. We have chosen to work with a rather than a' simply for convenience. Note that dose equilibrium is approached to within 2% on the peripheral axis (our central axis criterion) for $a'_{\mathrm{eq}}=L_{\mathrm{eq}}=300$ mm, and $a_{\mathrm{eq}}=400$ mm (compared to $L_{\mathrm{eq}}=a_{\mathrm{eq}}=470$ mm on the central axis).

III.D. Generating the complete data set for conventional and stationary phantom CT from a single measurement of the peak dose $f(0)$ resulting from a single axial rotation—An example

For added clarity, the peak axial profile dose $f(0)$ is parametrized in the following with the aperture a (primary beam width) as $f(0)_a$ and the experimental data of Mori[1] for a 32 cm diameter PMMA body phantom are utilized. We will presume for illustrative purposes that only a single measurement of $f(0)_a$ has been made at a single aperture setting a, using a single axial rotation about a small ion chamber (e.g., a Farmer-type chamber) in a stationary phantom. The strategy is then to determine the value of A_{eq} by inverting the relation

$$f(0)_a=H(a)A_{\mathrm{eq}} \tag{21}$$

and applying the analytical functions derived for $H(a)$ in Eqs. (16) and (19). Having obtained A_{eq}, we can then predict the desired stationary phantom dose $f(0)_a$ for any aperture a from Eq. (21) for the wide cone beams of SCBCT and the narrow fan beams of perfusion studies (or for any procedures using a stationary phantom).

But recall, we also showed that the same equilibrium dose A_{eq} applies to conventional axial or helical CT using phantom/table motion for a scan interval $b=\hat{a}$ or a pitch $p=\hat{a}/nT$. Thus, we can parlay the peak dose $f(0)_a$ value acquired using a single axial rotation about a stationary phantom with a conventional short ion chamber into the conventional CT equilibrium dose D_{eq} attained for any aperture setting $\hat{a}$ (any nT) for any table increment b (or any pitch

TABLE III. Stationary phantom doses $f(0)_a$, as predicted from a measurement of peak dose for a single aperture setting. In this example, $f(0)_{111}$ was used as the measured value (shown in bold type) from which the values of A_{eq} shown in the last row were predicted using $H(a)$. Predicted doses are given in *italics*, the actual measured doses (Ref. 1) from Tables I and II are also listed for comparison, and the % error is shown.

	Central axis				Peripheral axis			
		Peak dose $f(0)_a$				Peak dose $f(0)_a$		
a (mm)	Eq. (16) $H(a)$	Predicted $H(a)A_{eq}$	Measured Table I	Error (%)	Eq. (19) $H(a)$	Predicted $H(a)A_{eq}$	Measured Table II	Error (%)
138	0.715	*4.35* mGy	4.37 mGy	0.5	0.873	*9.38* mGy	9.60 mGy	−2.3
111	0.641		**3.90**		0.84		**9.02**	
49	0.385	*2.34*	2.27	3.1	0.714	*7.67*	8.06	−5.1
28[a]	0.272	*1.63*	1.53	8.0	0.630	*6.74*	7.34	−9.0
7.8	0.140	*0.85*			0.490	*5.26*		
∞	1.000	A_{eq}=*6.08*	A_{eq}=6.17	1.5	1.000	A_{eq}=*10.7*	A_{eq}=10.9	−1.5

[a]28 mm rounded off from 27.5 mm.

$p=b/nT$) using $D_{eq}=(\hat{a}/b)\,A_{eq}$, and thence the dose for any scan length L from $D_L(0)=H(L)\,D_{eq}$ using the same function expressed as $H(L)$; the complete data set from a single axial rotation without ever scanning over L.

From an experimental point of view, it would be better to use several (N) rotations and measure $Nf(0)_a$ (particularly on the peripheral axis) in order to minimize errors due to "end effects" (beam-on/off ramp-up times and variable start/stop angles); the extra acquisition time required is only seconds and inconsequential.

The following example using the data of Mori[1] in Tables I and II for the central and peripheral axes of the body phantom, respectively, will be used to illustrate the feasibility of this somewhat ambitious plan. It is assumed that the scanner can be operated in both a conventional CT mode as well as the SCBCT mode. The key to success is an accurate determination of A_{eq} which suggests using a reasonably wide beam, such as $a=111$ mm. We therefore presume that only a single measurement of the peak axial dose $f(0)_a=f(0)_{111}$ is made on each phantom axis, these being the values shown in bold type in Table III for $a=111$ mm. We will then attempt to predict the other data from these [and then check our predictions (shown in italics) against the actual measured data]. This is best illustrated by displaying the results in tabular form as in Table III.

The value of the aperture-independent constant A_{eq} is *predicted* using the measured peak dose for $a=111$ mm using $A_{eq}=f(0)_a/H(a)=f(0)_{111}/H(111)=3.90/0.641=6.08$ mGy on the central axis, and $A_{eq}=9.02/0.84=10.74$ mGy on the peripheral axis, which agree (within 1.5%) with the average experimental values of 6.17 and 10.86 from Tables I and II. Thence the value of the stationary phantom peak dose $f(0)_a=H(a)A_{eq}$ can be predicted for any aperture a, and some representative values are given in Table III for comparison with the measured values where available.

It might also be prudent to measure $f(0)_a$ for several values of a, since the additional acquisition time is minimal and of little consequence, and likewise to measure a $CTDI_L$ to confirm a good crossover. The doses for a narrow aperture of $a=7.8$ mm ($nT=5$ mm) such as one might use in a stationary phantom perfusion study are also shown in Table III, to illustrate that $CTDI_{100}$ overestimates the peak dose $f(0)$ by factors of 6.9 and 2.7 on the central and peripheral axes, respectively, and the reported $CTDI_{vol}$ (Ref. 13) overestimates the peripheral axis peak dose (comparable to the skin dose and pertinent to perfusion studies) by a factor of 4.1 (see Ref. 15).

This is not surprising since $CTDI_{100}$ represents the dose at the center of 20 contiguous 5 mm axial scans spaced at $b=nT=5$ mm, and thus includes significant scatter from the adjacent slices and over-beaming as well.

III.D.1. Crossover to conventional CT dose

We can also extend this single measurement of the SCBCT peak dose $f(0)_{111}$ to conventional CT and generate complete dose tables for that modality. We already have the predicted value of the quantity of greatest interest (and the most difficult to measure) in helical or axial scanning, namely, the equilibrium dose constant A_{eq} (with predicted values of 6.08 and 10.7 mGy from Table III), which have the same value for conventional CT (assuming the same bow-tie filter) and from which the conventional CT equilibrium dose D_{eq} for any table increment b (or any pitch $p=b/nT$) and for any aperture $\hat{a}$ (or nT) can be obtained using $D_{eq}=(\hat{a}/b)\,A_{eq}=(\hat{a}/nT)p^{-1}A_{eq}$, and thence the dose for any scan length L can be obtained using $D_L(0)=H(L)\,D_{eq}$. For example, assuming the scanner is operated in a helical mode with $nT=64\times0.5$ mm=32 mm (corresponding to an aperture $a=49$ mm), pitch $p=0.78$, $\tau=1$ s, total beam-on time $t_0=4.0$ s, scan length $L=vt_0=100$ mm; then $D_{eq}=(a/b)A_{eq}=(a/nT)p^{-1}A_{eq}=1.96A_{eq}=11.9$ and 21.0 mGy on the central and peripheral axes, respectively, which, when corrected to $L=100$ mm using the values of $H(L)=0.60$ from Eq. (17) and $H(L)=0.86$ from Eq. (20), results in dose values of $D_L(0)=H(L)D_{eq}=7.1$ and 18.1 mGy on the two axes.

IV. SUMMARY AND CONCLUSIONS

- For SCBCT scanning (without table/phantom motion), it was shown that the peak dose $f(0)$ on the central ray

($z=0$) of the cone beam is the logical (and unique) choice for a SCBCT dose-descriptor consistent with the CTDI-based dose used in conventional CT.

- This point dose $f(0)$ can be directly measured using a single axial rotation about a small ion chamber located in the phantom on the central ray of the primary beam ($z=0$).
- A common measurement method can be utilized for both the stationary and moving phantom, viz., a conventional, short ionization chamber (such as a 0.6 cc Farmer-type chamber) located at the center $z=0$ of the directly irradiated length to measure the dose $Nf(0)$ for SCBCT, or the accumulated dose $D_L(0)$ at $z=0$ in conventional CT using a helical (or axial) scan series[2] to translate the phantom (and ion chamber) over $(-L/2, L/2)$ where $L=vt_0$ (or $L=Nb$). This direct measurement method is actually more general than the theoretical equations, requiring neither shift-invariance of the phantom, the x-ray beam, nor the scan interval.
- The equilibrium dose constant $A_{eq}=(b/a)D_{eq}$ is independent of both pitch $p=b/nT$ and aperture a (thence nT), and was shown to have a common value for both SCBCT and conventional CT, and its constancy has been demonstrated over a wide aperture range ($28\ \text{mm} \leq a \leq 138\ \text{mm}$); therefore it is sufficient to determine A_{eq} at a single known aperture value a (which need not be a wide beam).
- Many common features of the SCBCT dose $f(0)$ as a function of cone beam width a and the conventional CT dose $D_L(0)$ as a function of scan length L have been established, including a common equilibrium dose constant A_{eq}, a common scatter equilibrium length $a_{eq}=L_{eq}$, and a common function $H(\lambda)$ which describes the relative approach to dose equilibrium for both modalities, where $\lambda=a$, or $\lambda=L$, such that $f(0)_a=H(a)A_{eq}$, and $D_L(0)=H(L)D_{eq}=H(L)(b/a)A_{eq}$.
- Using the scatter LSF derived from the Monte Carlo simulation of Boone,[17] analytic functions describing the variation in the peak dose of an axial dose profile $f(0)_a$ and $H(a)=f(0)_a/A_{eq}$ as a function of collimator aperture a (primary beam width) were derived [e.g., see Eqs. (15) and (16)], which functions provided a good match to the experimental data,[1,2] and which have importance and utility for predicting the peak dose for the narrow fan beams used in perfusion studies[15] as well as the relevant cone beam dose $f(0)$ in SCBCT for any beam width (aperture) a.
- The commonality described above also suggests the possibility that a single measurement of the peak dose $f(0)_a$ of an axial dose profile resulting from a single rotation about a stationary phantom for a single (arbitrarily chosen) aperture a setting using a small ion chamber is sufficient to predict the peak dose $f(0)_a$ for any other aperture, for wide cone beams and narrow fan beams alike, including the scatter equilibrium dose constant A_{eq} using the function $H(a)$ to obtain $A_{eq}=f(0)_a/H(a)$. The value of A_{eq} can then be used to predict the equilibrium dose D_{eq} for conventional axial or helical CT scans for any table increment b (or any pitch $p=b/nT$) at any aperture setting a (any nT) using $D_{eq}=(a/b)\ A_{eq}$, and thence to predict the dose for any desired subequilibrium scan length L using $D_L(0)=H(L)\ D_{eq}$ using the same analytical function $H(\lambda)$ with $\lambda=L$; obtaining the complete data set without ever scanning over L. That is, the theory developed allows a "crossover" between stationary phantom and conventional (helical or axial) scanning modalities (assuming shift-invariance exists). In fact, one obtains the complete data set for both modalities, namely, $f(0)_a$ for any a, A_{eq}, $D_{eq}=(a/b)\ A_{eq}$, and $D_L(0)$ for any L, all from a single measurement of the peak dose $f(0)_a$ of an axial dose profile resulting from a single axial rotation about a stationary phantom.
- Inspection of Fig. 3 illustrates the rather remarkable confluence of an analytical, theoretical function based on a scatter LSF obtained from a Monte Carlo simulation, with axial profile peak doses $f(0)_a$ measured on a Toshiba 256 channel cone beam scanner, with helical scan doses $D_L(0)$ measured on conventional GE LS scanners, which speaks to the generality of these results.
- This work is based on Monte Carlo data[17] obtained at 120 kVp in a 32 cm diameter PMMA phantom using a typical bow-tie filter, and is intended as a proof of concept exposition (which successfully matched the experimental data[1,2]); moreover, the theory and equations are quite general and can now be easily extended[17] to any phantom diameter (for a variety of phantom materials) at a variety of kVp settings (with or without) bow-tie filters; and these systematics are to be developed in future work. It would also be useful to have further corroborative experimental measurements of peak doses $f(0)_a$ for narrow axial profiles in the range of ($5\ \text{mm} \leq nT \leq 40\ \text{mm}$).

ACKNOWLEDGMENTS

The authors are grateful to Dr. Shinichiro Mori for supplying the numerical beam profile data for the various cone beam widths for the prototype 256 channel scanner as previously published in Medical Physics (Ref. 1).

NOMENCLATURE

MDCT	=	"Multidetector CT"
Fan beam	=	A nominal beam width of $\leq$40 mm along z ($\geq$40 mm is typically called a cone beam)
Shift-invariance	=	Translational invariance (independent of location along the z-axis)
AOR	=	Gantry axis of rotation located at isocenter; F=source to isocenter distance
t_0	=	Total beam-on time for an axial or helical scan series (tube loading time)

τ = Time for a single 360° gantry rotation (typically $\tau=1$ s or less)
N = (t_0/τ)=total number of gantry rotations in an axial or helical scan series (N may not be an integer for helical scanning)
v = Table velocity for helical scans
b = Generalized table advance per rotation (mm/rot), or *table index*
b = $v\tau$ for helical scans; b=scan interval for axial scans (denoted elsewhere as Δd or "I")
L = vt_0=definition of total helical scan length (the total reconstructed length is $<L$)
L = Nb=generalized definition of total scan length (axial or helical)
$\Pi(z/L)$ = rect function of unit height and width L spanning an interval $(-L/2, L/2)$
nT = Total slice width acquired in a single rotation (often denoted by "$N\times T$"). Also equal to the total active detector length projected at isocenter for MDCT (e.g., $nT=16\times 1.25$ mm=20 mm)
a = Geometric projection of the z-collimator aperture onto the AOR (by a "point" focal spot). For MDCT $a>nT$ (called "overbeaming") to keep the penumbra beyond the active detector length nT
p = b/nT=generalized "pitch"
Accumulated dose = Dose accrued at a given z (e.g., $z=0$) due to a complete series of N axial or helical rotations
$f(z)$ = Single rotation (axial) dose profile acquired with the phantom held stationary
D_{eq} = Limiting value of accumulated dose approached in conventional CT for scan lengths $L\geq L_{eq}$
L_{eq} = Scan length required for the dose to approach to within $<2\%$ of D_{eq} at $z=0$ (denoted symbolically as $L\rightarrow\infty$)
A_{eq} = The equilibrium dose constant, equal to D_{eq} for a table increment $b=a$ (and independent of aperture a and nT)
R = Radius of cylindrical phantom
η = Scatter to primary ratio S/P

APPENDIX A: DERIVATION OF THE LSF FORMULATION FOR THE PERIPHERAL AXIS

By analogy with Eq. (7)

$$f(z,\theta)=A_0(\theta)\left[\frac{1}{c(\theta)}g\left(\frac{-z}{c(\theta)}\right)+\eta(\theta)\mathrm{lsf}(z,\theta)\right]\otimes\Pi\left(\frac{z}{a(\theta)}\right), \tag{A1}$$

where $A_0(\theta)=f_p(0,\theta)$ is the primary beam intensity (dose rate) on the peripheral axis, and is thus the appropriate weighting function to average various parameters over θ as related to the peripheral axis.[5] For example, the average of $A_0(\theta)a(\theta$ can be written as $A_0\langle a\rangle$ where $A_0=f_p(0)$ is the *total* primary beam dose on the peripheral axis [the integral of $A_0(\theta)=f_p(0,\theta)$ over all angles[5]], and $\langle a\rangle$ is the dose-weighted average of the projected aperture $a(\theta)$ on the peripheral axis, which is equal to the width (FWHM) of the primary beam profile $f_p(z)$ on that axis. The presence of $a(\theta)$ in the rect function $\Pi[z/a(\theta])$ in Eq. (A1) breaks the shift-invariant symmetry required by the convolution once the integration over θ is performed. Expressing the convolution in Eq. (A1) in its integral form, illustrates the difficulty, namely,

$$f(z,\theta)=A_0(\theta)\left[1+\int_{-a(\theta)/2}^{a(\theta)/2}\mathrm{LSF}(z-z',\theta)dz'\right]. \tag{A2}$$

Fortunately the problem is solvable in closed form on the peripheral axis, since most of the dose on a given peripheral axis is contributed while the beam is directly incident on that axis ($\theta=0$), due to the fact that phantom, bow-tie filter, and secondarily inverse square attenuation[5] serve to rapidly "pinch off" the primary beam intensity $A_0(\theta)$ at angles beyond about $\pm 50°$, over which angular range $a(\theta)$ is slowly varying. This likewise applies to the peripheral axis of the head phantom,[5] where the roll off of $A_0(\theta)$ is slower, but which is compensated by a smaller variation in $a(\theta)$. In fact, it was previously shown[5] that $\langle a\rangle=1.05\ a(0)$ for the peripheral axes in both body and head phantoms, and only 5% above its minimum value $a(0)$ at $\theta=0$. This limited variation in $a(\theta)$ allows one to replace it in the above equations by its average value $a'=\langle a\rangle$ with negligible error, thereby preserving the convolution format (a' is equal to the FWHM of the axial dose profile on the peripheral axis). Indeed, this approximation is good on a z-axis located at any radius in either phantom.

Replacing $a(\theta)$ by $a'=\langle a\rangle$ in Eq. (A2) and setting $z=0$ gives

$$f(0,\theta)=A_0(\theta)\left[1+\int_{-a'/2}^{a'/2}\mathrm{LSF}(z',\theta)dz'\right], \tag{A3}$$

which, when averaged (integrated) over θ, gives

$$\begin{aligned} f(0)&=A_0+\int_{-a'/2}^{a'/2}dz'\frac{1}{2\pi}\int_{-\pi}^{\pi}A_0(\theta)\mathrm{LSF}(z',\theta)d\theta \\ &=A_0+A_0\int_{-a'/2}^{a'/2}\langle\mathrm{LSF}(z')\rangle dz', \end{aligned} \tag{A4}$$

where $\langle\mathrm{LSF}(z')\rangle$ denotes the dose-weighted angular average of $\mathrm{LSF}(z,\theta)=\eta(\theta)\mathrm{lsf}(z,\theta)$ over a complete rotation.

Equation (A4) is seen to have the same form as Eq. (12) for the central axis [recognizing the scaled form of the LSF

previously used $\mathrm{LSF}(z)=\eta d^{-1}h(z/d)]$, thus Eq. (17) for $f(0)$ and Eq. (18) for $H(a)$ also apply, if one replaces a with the FWHM of the axial dose profile on the peripheral axis $a'=\langle a\rangle\approx 1.05a(0)\approx 0.76a$, where $a(0)=a(F-15\ \mathrm{cm})/F$, and where F is the focal to AOR distance, and uses the values of the (double-exponential) fit parameters $(\varepsilon,d,\delta d)$ appropriate to the peripheral axis and $\eta=1.5$.

[a]Electronic mail: rdixon@wfubmc.edu

[1]S. Mori, M. Endo, K. Nishizawa, T. Tsunoo, T. Aoyama, H. Fujiwara, and K. Murase, "Enlarged longitudinal dose profiles in cone-beam CT and the need for modified dosimetry," Med. Phys. **32**, 1061–1069 (2005).
[2]R. L. Dixon and A. C. Ballard, "Experimental validation of a versatile system of CT dosimetry using a conventional ion chamber: Beyond CTDI_{100}," Med. Phys. **34**(8), 3399–3413 (2007).
[3]R. L. Dixon, "A new look at CT dose measurement: Beyond CTDI," Med. Phys. **30**, 1272–1280 (2003).
[4]T. Shope, R. Gagne, and G. Johnson, "A method for describing the doses delivered by transmission x-ray computed tomography," Med. Phys. **8**, 488–495 (1981).
[5]R. L. Dixon, M. T. Munley, and E. Bayram, "An improved analytical model for CT dose simulation with a new look at the theory of CT dose," Med. Phys. **32**, 3712–3728 (2005).
[6]R. L. Dixon, "Restructuring CT dosimetry—A realistic strategy for the future. Requiem for the pencil chamber," Med. Phys. **33**, 3973–3976 (2006).
[7]U.S. FDA, "Performance standards for diagnostic x-ray systems," Fed. Regist. 49(171), Computed Tomography (CT) equipment, Section 33, pp. 646–651 (1984).
[8]J. M. Boone, V. N. Cooper III, W. R. Nemzek, J. P. McGahan, and J. A. Seibert, "Monte Carlo assessment of computed tomography dose to tissue adjacent to the scanned volume," Med. Phys. **27**, 2393–2407 (2000).
[9]W. Leitz, B. Axelson, and G. Szendro, "Computed tomography dose assessment—A practical approach," Radiat. Prot. Dosim. **57**, 377–380 (1995).
[10]K. D. Nakonechny, B. G. Fallone, and S. Rathee, "Novel methods of measuring single scan dose profiles and cumulative dose in CT," Med. Phys. **32**, 98–109 (2005).
[11]H. T. Morgan and R. Luhta, "Beyond CTDI dose measurements for modern CT scanners," Med. Phys. **31**(6), 1842 (2004); H. T. Morgan and R. Luhta, personal communication (2004).
[12]J. Anderson, D. Chason, G. Arbique, and T. Lane, "New approaches to practical CT dosimetry," Med. Phys. **32**, 1907 (2005).
[13]International Standard IEC 60601–2-44, "Particular requirements for the basic safety and essential performance of x-ray equipment for computed tomography," *Medical Electrical Equipment—Part 2–44*, Edition 3.0 (International Electrotechnical Commission, Geneva, Switzerland, 2009).
[14]R. N. Bracewell, *The Fourier Transform and Its Applications*, 3rd ed. (McGraw-Hill, Boston, 2000).
[15]J. A. Bauhs, T. J. Vrieze, A. N. Primak, M. R. Bruesewitz, and C. J. McCollough, "CT dosimetry: Comparison of measurement techniques and devices," Radiographics **28**, 245–253 (2008).
[16]J. M. Boone, "The trouble with CTDI_{100}," Med. Phys. **34**, 1364–1371 (2007).
[17]J. M. Boone, "Dose spread functions in computed tomography: A Monte Carlo study," Med. Phys. **36**, 4547–4554 (2009).